

## Cyclic normal load–displacement behaviour of clay-coated sand grain contacts

SARVADEVABHATLA SATHWIK KASYAP\*, KOSTAS SENETAKIS† and JIDONG ZHAO‡

A micromechanical experimental study is presented in this paper investigating the normal contact response of quartz sand grains under cyclic loading. Sand grains with clean surfaces, termed uncoated, and grains coated with commercially available kaolinite powder were studied. The grain contacts were subjected to ten cycles of normal loading within a range from 0 to 5 N. It was observed that uncoated sand grains showed dominantly elastic behaviour, but coated particles had a gradual transition into elastic behaviour after significant plastic deformations in the initial cycles. The normal contact stiffness of coated particles initially increased notably with the number of cycles and reached a maximum value, but uncoated particles showed no variation of normal stiffness against the loading cycles. Similar trends were observed for the stiffness ratio against the loading cycles. Total work input required to reach a given maximum normal load along with elastic and plastic fractions of work input were calculated for coated particles. For uncoated particles, these values were negligibly low, and it was impractical to find elastic and plastic fractions precisely. For coated particles, with a lower preloading at 2 N, the normal load–displacement curve reaching 5 N deviated after a threshold value of 2 N was reached – that is after reaching the previous maximum load the grains contact had experienced. This effect was more pronounced with the increase of the cycles during preloading at 2 N. However, a preloading at 10 N – that is the grains were subjected to greater previous load prior to the normal load–displacement test at 5 N, caused a decrease in plastic deformations and increase in stiffness ratio in the subsequent cycle at 5 N. Uncoated grain contacts did not demonstrate notable variations under the preloading conditions.

**KEYWORDS:** discrete-element modelling; laboratory equipment; laboratory tests; stiffness

### INTRODUCTION

A significant enhancement of knowledge regarding the behaviour of soils has been achieved in recent years due to the development and implementation of the discrete-element method (DEM), first introduced by Cundall & Strack (1979), in a broad range of geotechnical engineering problems. A key step in a DEM analysis constitutes the calculation of forces between the contacted grains, which is influenced by the type of the materials in contact, their morphology and the specific load–displacement relationship implemented as the constitutive law at the grain contacts (O’Sullivan, 2011; Kawamoto *et al.*, 2018). Based on numerical results from the literature, it is well acknowledged that the inputs in a DEM model, which includes the implemented contact mechanics properties such as grain-contact stiffness and friction as well as the morphological characteristics of the grains, play a very important role in the expected output (e.g. Thornton, 2000; Yimsiri & Soga, 2000; Soga & O’Sullivan, 2010; Dai *et al.*, 2016; Huang *et al.*, 2017; Otsubo & O’Sullivan, 2018). This has encouraged more systematic studies to be conducted in

the laboratory in recent years to quantify the properties of real soil grain contacts (Cole & Peters, 2007, 2008; Cavarretta *et al.*, 2010; Senetakis *et al.*, 2013; Cole & Hopkins, 2016; Nardelli *et al.*, 2017). This can enhance the fundamental understanding of the dominant mechanisms that control grain contact behaviour and it also provides useful parameters to be further utilised in DEM simulations.

In both monotonic and cyclic loading, as well as dynamic problems of granular materials, it is important to understand how forces and displacements interact at the grain contacts under cycles of increased and decreased magnitudes of applied load. Previous works on the cyclic behaviour of granular materials using DEM emphasised the importance of the inter-particle friction on the stress–strain behaviour and energy dissipation (Sazzad & Suzuki, 2011); however, the underpinning role of the implemented normal load–displacement relationship has largely been overlooked. Based on the micromechanical experimental works by Sandeep & Senetakis (2018a) and Sandeep *et al.* (2018), it has been concluded that the grain contact response can be highly elastic or dominantly plastic depending upon the material type. The normal load–displacement (as well as the tangential load–displacement) relationship to be implemented in a DEM study should therefore take into account the specific problem to be considered – that is the type of material that is intended to be tested, which in turn can influence markedly the mechanical responses at the grain contact level.

In this paper, a laboratory study is presented to investigate the role of cyclic loading in the normal contact behaviour of pairs of sand grains. Two types of contacts are examined, including Leighton Buzzard sand (LBS) quartz grains, as well as LBS grains coated with kaolinite powder. Coated grains are examined in the study to understand how the contact responses may be affected in the presence of a soft

Manuscript received 1 September 2018; revised manuscript accepted 31 October 2019. Published online ahead of print 6 December 2019. Discussion on this paper closes on 1 July 2021, for further details see p. ii.

\* Department of Architecture and Civil Engineering, City University of Hong Kong, Kowloon, Hong Kong SAR, P. R. China.

† Department of Architecture and Civil Engineering, City University of Hong Kong, Kowloon, Hong Kong SAR, P. R. China (Orcid:0000-0003-0190-4768).

‡ Department of Civil and Environmental Engineering, Hong Kong University of Science and Technology, Hong Kong SAR, P. R. China.

material at sand grain contacts, subjected to a number of loading-unloading cycles. There are applications in the field of sand grain contacts in the presence of a coating agent of micro-particles, for example in sedimentary soil mixtures, weathered rock profiles or compacted fills/backfills/embankments. Research works related to the effects of soil mixtures (i.e. sand-silt-clay combinations) on the frictional and strength characteristics using macro-scale tests are available (Yang & Wei, 2012; Phan *et al.*, 2016). Few works related to the formation of coating on geological materials, either naturally or artificially, are available. Scheidegger *et al.* (1993) worked on coating silica sand with goethite (iron oxide compound), introducing various coating techniques. Barrows *et al.* (1966) studied the formation of a natural coating of aluminium, phosphorous and manganese on limestone in soil. In the field of micromechanics, few works on artificially cemented grains are found which could be considered as coatings that strongly bond the grains (Wang *et al.*, 2017, 2018). Micromechanical studies and works related to contact mechanics of clay-coated sands are still unexplored. Principally, the work looks at a more fundamental level of the normal contact behaviour of coated grains, so that the coating has been applied in a controlled manner to achieve the reproducibility of the grains in consideration. Kasyap & Senetakis (2018) presented this new technique of coating sand grains and, subsequently, preliminary micromechanical test results in terms of monotonic behaviour to provide a general indication of the influence of coating. This coating technique and some insights on the micromechanical behaviour of coated sands has become a basis for the present study on the cyclic normal load behaviour. Emphasis is placed on the work done and the distinction between elastic and plastic portions, the normal stiffness and the role of the number of loading cycles, as well as the influence of loading history in terms of preloading; here 'preloading' refers to the previous maximum load that a contact has been subjected to compared with the current normal load.

## MATERIALS, EQUIPMENT AND TESTING PROGRAMME

Leighton Buzzard sand quartz grains of 2.36–5.00 mm in size were used in this study. These grains are sub-rounded to rounded, yellow to brown in colour with a greasy lustre on their surfaces. Two classes of LBS grains were tested in the present study: (a) LBS (i.e. the grains were uncoated and cleaned from any dust or impurities on their surfaces) and (b) coated LBS (i.e. artificially coated grains with commercially available kaolinite powder). The coating of the LBS grains was achieved by suspending the sand particles in a kaolinite solution of a given concentration. Using an orbital shaker, the kaolinite solution with sand grains was thereafter vibrated for a specified period of time. The class of type-H particles, as described in Kasyap & Senetakis (2018), was used for the micromechanical tests along with the LBS particles. This class corresponds to a relatively heavier amount of coating material, which results in a substantial increase of the aluminium (Al) element on the surfaces of the grains compared with the relatively small aluminium content found on LBS. The surface roughness ( $S_q$ ) values for LBS and type-H particles was quantified using a surface profiler of the Veeco NT9300 type on a representative set of grains.  $S_q$ , as an average value  $\pm$  one standard deviation, corresponded to  $223 \pm 61$  nm for LBS (after Sandeep & Senetakis (2018b)) and  $1013 \pm 140$  nm for type-H particles (after Kasyap & Senetakis (2018)). The micro-hardness value of type-H particles was found to be equal to  $2.5 \pm 0.9$  GPa based on tests using the Fischer-scope HM2000 micro-hardness tester. For LBS, Todisco *et al.* (2017) found an

average value of 6.2 GPa. The flaky particles of kaolinite adhered on the surface of the LBS grains increase the surface roughness, but because of their softer nature, the coated grains had markedly lower values of micro-hardness as compared to LBS.

A custom-built micromechanical loading apparatus, which has been described by Senetakis & Coop (2014) and Nardelli & Coop (2018), was used in the study (Fig. 1(a)). The apparatus consists of linear micro-stepping motors, high-resolution load cells ( $\pm 0.02$  N) and non-contact displacement sensors ( $\pm 0.01$   $\mu$ m); these are assembled in three perpendicular directions and are connected with stiff mechanical parts and bearing systems of minimum friction, which makes the apparatus highly competent for grain-scale mechanical tests. Additionally, a high-quality data logging system and analogue filters, as described by Senetakis & Coop (2014), are used to provide adequate quality of output data. Technical data and calibration details of the apparatus, as well as its repeatability in testing reference grains and experiments on a broad range of geological materials, including both uncemented and cemented sand grains, have been reported in recent studies (e.g. Senetakis *et al.*, 2013; Nardelli *et al.*, 2016, 2017; Wang *et al.*, 2017; Nardelli & Coop, 2018; Sandeep *et al.*, 2018; Sandeep & Senetakis, 2019). This apparatus is so designed that the interface responses of two sand-sized grains in terms of normal and tangential load against displacement can be examined to resolve and quantify inter-particle friction and contact stiffness.

In the study, both LBS and type-H particles were tested under cyclic normal load with ten loading cycles. Figs 1(b) and 1(c) show LBS and type-H particles fixed in the apparatus for testing. It is noted that one cycle corresponds to an increase of the normal load,  $F_N$ , from zero to a desired maximum value, followed by unloading back to zero  $F_N$ , considering that the grains cannot transfer a tensile load at their contact. The emphasis of the study is placed on the quantification of the elastic and plastic deformations, and the corresponding work input required at the contacts of the grains and their relationship with the number of loading cycles, the normal contact stiffness, the stiffness ratio variation with the number of cycles and the effect of preloading on the behaviour of the grains. The definitions of these parameters are explained in their respective sections later in this paper. Fig. 2 provides an explanation of the various parameters studied here using a typical load-displacement curve of type-H particles as an example. From each class of grains, three different pairs of grains were tested to assess the overall repeatability of the results. The total set of six experiments is summarised in Table 1. For test numbers 1 and 2, ten loading cycles were applied at a maximum  $F_N$  of 5 N (i.e. each cycle reached a maximum load of 5 N). For tests from number 3 to number 6, one cycle of normal load at  $F_N = 5$  N was applied, but prior to this, a preloading was conducted at 2 or 10 N with one to five cycles, as summarised in Table 1. Based on this testing programme, the emphasis was placed on the normal load-displacement behaviour at a maximum load of 5 N accounting for the number of loading cycles as well as the previous loading history at the same (i.e. 5 N) or different (i.e. 2 or 10 N) magnitude of  $F_N$ . All the tests were conducted by force control at a rate of 30 N/h for both loading and unloading phases.

## RESULTS AND DISCUSSION

### Elastic and plastic deformations

The total deformation ( $\delta_{\text{total}}$ ) required to reach a given maximum load can be divided into elastic ( $\delta_{\text{elastic}}$ ) and plastic

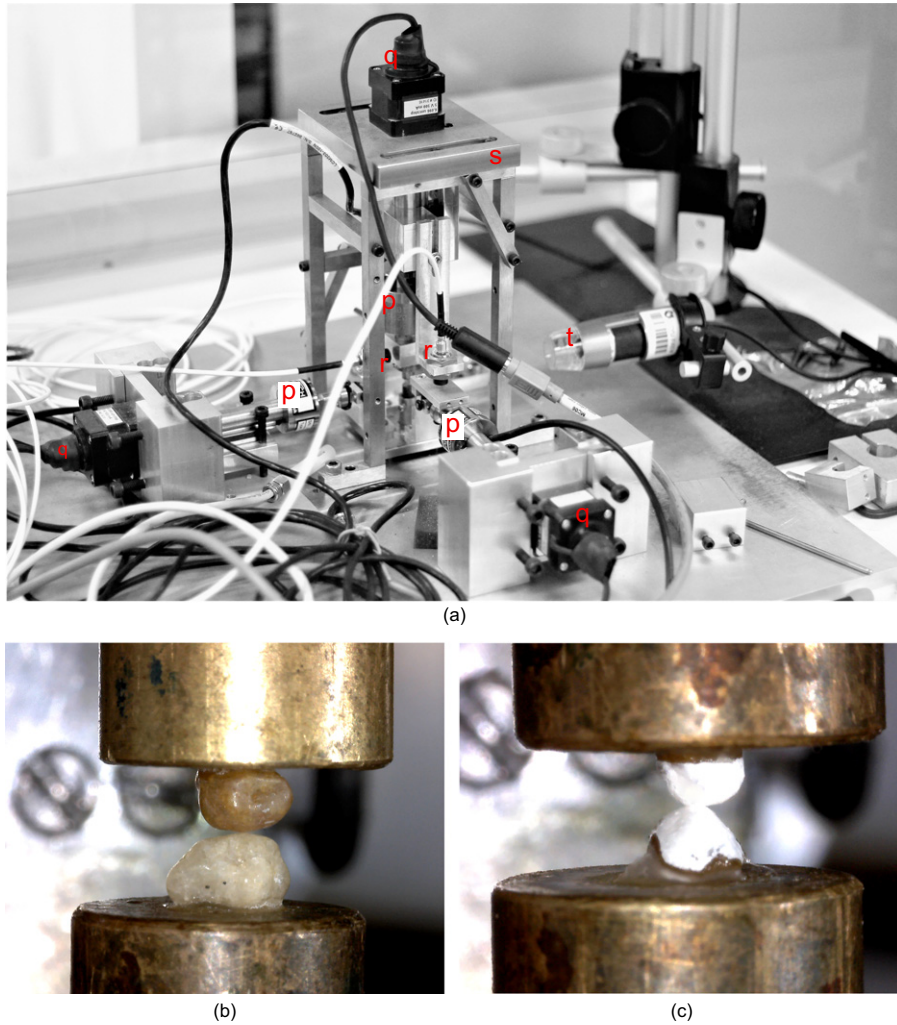


Fig. 1. (a) Micromechanical loading apparatus developed at City University of Hong Kong (p, load cells; q, micro-stepper motors; r, non-contact displacement sensors; s, rigid frame; t, micro-camera). (b) LBS grains and (c) type-H particles fixed with peak-to-peak contact

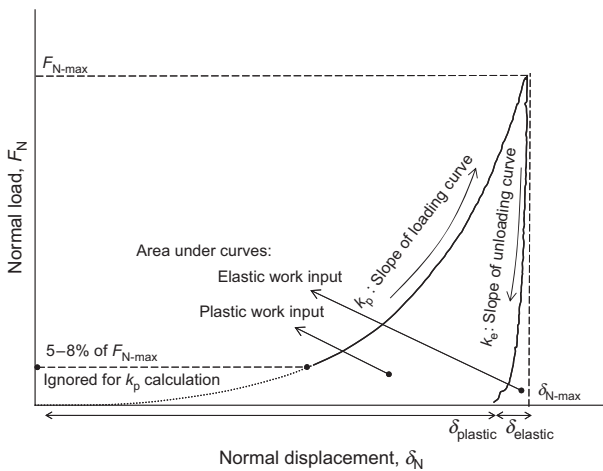


Fig. 2. Pictorial explanation of various terms related to analysis of cyclic normal load tests

( $\delta_{plastic}$ ) counterparts.  $\delta_{elastic}$  and  $\delta_{plastic}$  are the recovered and unrecovered displacements, respectively, after one cycle of loading–unloading (see Fig. 2). Figs 3(a) and 3(b) show the cyclic normal load–displacement behaviour of both type-H particles and LBS, respectively, with a maximum normal load of 5 N for ten cycles. The insets of the figures show the

Table 1. Details of testing programme

Test no.	Particle type	Preloading condition		$F_{N,max}$ : N	Cycles
		Load: N	Cycles		
1	Type-H	—	—	5	10
2	Pure LBS	—	—	5	10
3	Type-H	2	1	5	1
4	Type-H	2	5	5	1
5	Type-H	10	1	5	1
6	Pure LBS	2	1	5	1

variation of  $\delta_{elastic}$  and  $\delta_{plastic}$  fractions from cycle to cycle and also the change of  $\delta_{total}$  as an absolute value. It was observed that for type-H particles the first cycle of loading displayed a high  $\delta_{plastic}$  of 23.2  $\mu m$ , which corresponded to 90% of  $\delta_{total}$  (25.8  $\mu m$ ). This plastic deformation is attributed to the permanent damage of the asperities (i.e. coating material) on the surface of type-H particles. In the second cycle,  $\delta_{plastic}$  dropped down to 4.6  $\mu m$  and the  $\delta_{plastic}$  fraction decreased to 54% of  $\delta_{total}$ . This decrease in  $\delta_{total}$  and  $\delta_{plastic}$  fraction continued throughout the total set of ten cycles, but the degradation (i.e. the decrease of  $\delta_{plastic}$  fraction and the absolute magnitude of  $\delta_{total}$ ) was faster in the first four to five cycles. After ten cycles of loading,  $\delta_{total}$  became so small that

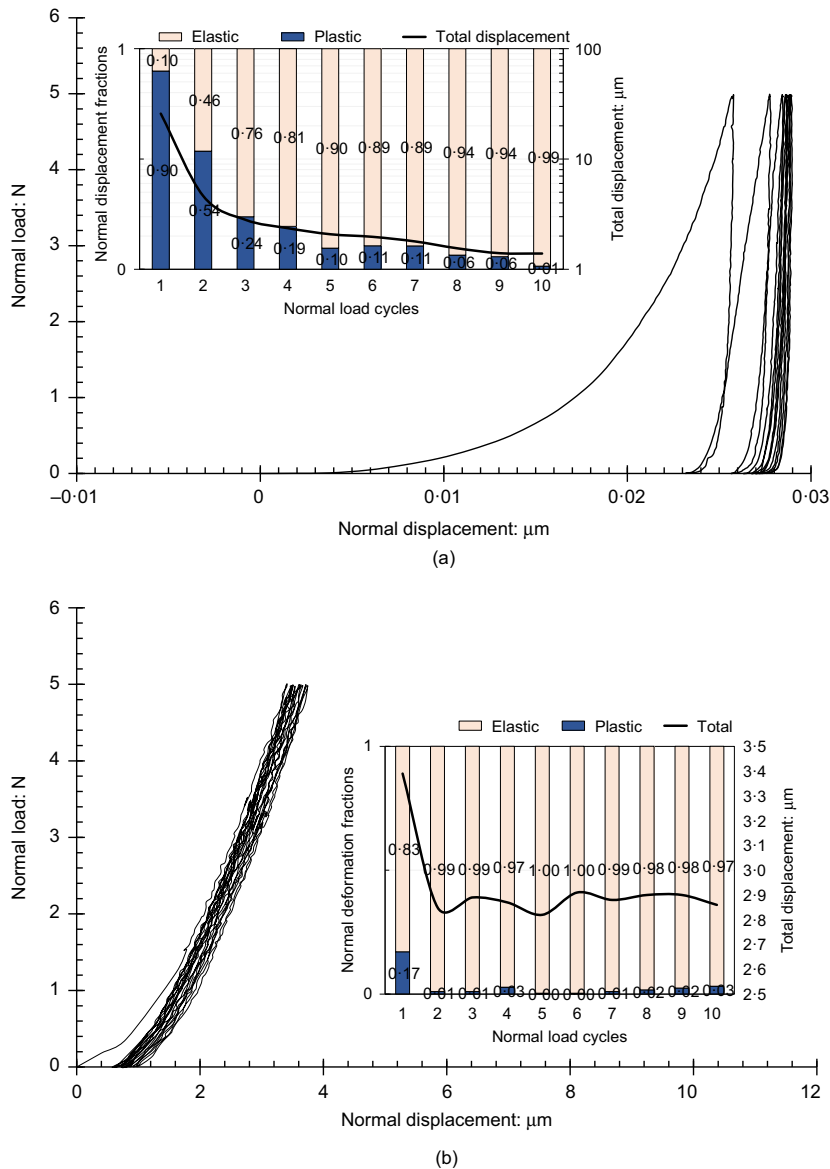


Fig. 3. Representative cyclic normal load–displacement curves applying 5 N of maximum normal load for 10 cycles: (a) type-H; (b) LBS. Insets of the figures show the fractions of elastic and plastic deformations for each cycle and the change of the total displacement with the number of cycles

the total displacement was almost recovered after unloading. For LBS particles, the behaviour was predominantly elastic with only 17% of  $\delta_{\text{plastic}}$  in cycle 1 (as a fraction of  $\delta_{\text{total}}$ ), which further reduced to about 1–3% in the consecutive cycles. The change in  $\delta_{\text{total}}$  from cycle 2 was vanishingly small and its variation was random within a narrow range of displacements (about  $\pm 0.1 \mu\text{m}$ ). It can be observed that, for the subset of Fig. 3(a), a logarithmic scale was used for the  $\delta_{\text{total}}$  axis considering the high range of variation in  $\delta_{\text{total}}$  for type-H particles (around  $24 \mu\text{m}$ ) after ten cycles, unlike LBS particles ( $0.6 \mu\text{m}$ ).

The damage on surfaces of LBS grains was not distinguishable with microscopic images due to the smaller heights of peaks (lower surface roughness). A similar observation was made by Sandeep & Senetakis (2018a) for LBS grains with normal load up to 12 N. However, the coated particles showed significant damage due to abrasion of the coating surface and representative scanning electron microscopy (SEM) images of damaged particles after ten cycles of normal loading are shown in Fig. 4.

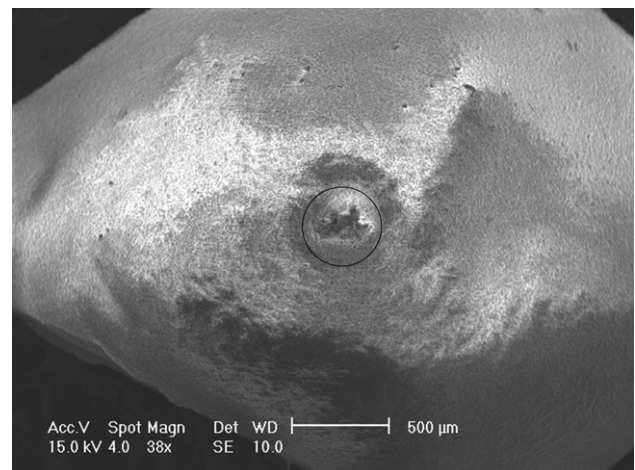
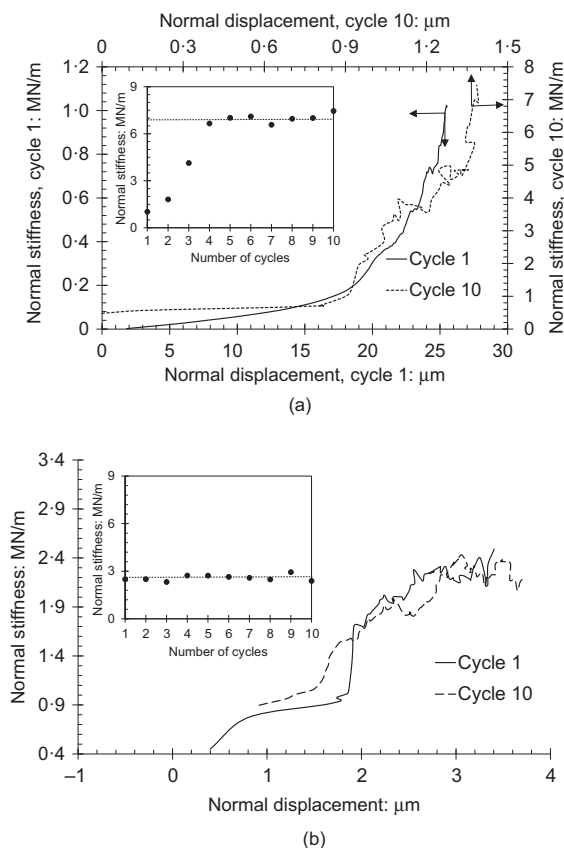


Fig. 4. SEM image showing the damage of coating surface after ten cycles of normal loading at 5 N  $F_{N-\text{max}}$

### Normal contact stiffness and stiffness ratio

Figures 5(a) and 5(b) show the variation of normal contact stiffness ( $K_N$ ) with normal displacement for type-H and LBS, respectively. Normal contact stiffness and displacement values corresponding to cycle 1 ( $K_{N1}^H$  and  $K_{N1}^{LBS}$  for type-H and LBS) and cycle 10 ( $K_{N10}^H$  and  $K_{N10}^{LBS}$  for type-H and LBS) were used in primary (bottom and left) and secondary (top and right) axes, respectively. Insets of Fig. 5 show the variation of peak  $K_N$  values observed in each cycle. The stiffness values were calculated by numerical differentiation of the normal load–displacement data (Cole & Peters, 2008) for the loading phase. A local slope from four to eight data points of load and displacement on both sides of a given displacement, obtained from the test, was found using the ‘Linest’ function in a spreadsheet and the stiffness variation with displacement is plotted.  $K_{N1}^H$  values increased up to 1.1 MN/m at a displacement of 25.5  $\mu\text{m}$ , but the behaviour was much stiffer at the tenth cycle, with  $K_{N10}^H$  reaching a value of 7.5 MN/m at a displacement of 1.4  $\mu\text{m}$ . The much lower  $K_N$  value in the first cycle is attributed to the influence of the soft kaolinite particles in the contact region. The damage of coating in subsequent cycles – that is, kaolinite particles gradually being either removed and/or displaced and more reasonably, kaolinite particles being compressed between top and bottom particles increased the stiffness. This also produced much greater elastic deformations, compared to the plastic response, as well as lower absolute values of total displacements with the increase of cycle number, as described in the previous section. It was interesting to observe that the variation of  $K_N^H$  with the normal displacement showed two



**Fig. 5.** Comparison of normal contact stiffness–displacement variation for cycle 1 and cycle 10: (a) type-H (bottom and left axes – cycle 1; top and right axes – cycle 10); (b) LBS. Insets of figures show the variation of the peak normal contact stiffness with the number of cycles

different trends. For both cycle 1 and cycle 10, there was a very slight variation of stiffness for displacements up to 40–50% of  $\delta_{\text{total}}$ , but  $K_N$  increased rapidly for displacements beyond about half of  $\delta_{\text{total}}$ . With the number of cycles, the  $K_N^H$  value increased up to the third applied cycle and, thereafter, showed an average value of 6.97 MN/m. The uniform stiffness in the initial stages of displacement can be attributed to the compression of soft coating material, more compression in cycle 1 (~15  $\mu\text{m}$ ) than in cycle 10 (0.8  $\mu\text{m}$ ). Looking into the total displacement variation with number of cycles for type H particles, as shown in the inset of Fig. 3(a), after cycle 4 not much variation in the total displacement was found and hence the stiffness values were uniform. For LBS particles, the variation of  $K_N$  with the number of cycles was almost negligible. An average value of 2.58 MN/m was observed through ten cycles of loading. Cole & Hopkins (2016) reported  $K_N$  of 2.0 MN/m for quartz sands. The randomness observed from cycle to cycle can be attributed to the small range of displacement values for LBS. Although type-H particles had lower stiffness than LBS in the initial cycles, in subsequent cycles the coated grain contacts reached about three times greater stiffness compared with LBS. This can be attributed to the compression of heavy debris formed from kaolinite between the particles.

In Luding’s linear model for elasto-plastic and adhesive contacts (Luding, 2008) and also in Walton and Johnson’s linear model (Walton & Johnson, 2009), the rate at which contact force increases in normal loading was termed as plastic stiffness ( $k_p$ ) and the unloading rate was termed as elastic stiffness ( $k_e$ ). Although the normal load–displacement behaviour for type-H and LBS particles is non-linear, the average slope of the load–displacement curve in loading ( $k_p$ ) and unloading ( $k_e$ ) phases is considered for analyses, adopting the terminology of Walton & Johnson (2009). As shown in Fig. 2, the initial very high non-linear part (up to 5–8% of  $F_{N-\text{max}}$ ) of the load–displacement curve is excluded from the calculation of slope for approximate linearity. The stiffness ratio is the ratio of elastic stiffness to plastic stiffness ( $k_e/k_p$ ) and is used to compare the influence of elastic and plastic deformations in a given cycle of loading (Pasha *et al.*, 2014). These terms are explained with an example load–displacement curve in Fig. 2. Fig. 6 shows the variation of stiffness ratio with number of cycles for both type-H and LBS. For type-H, it was observed that the stiffness ratio has a very high value for cycle 1 for type-H, which explains the higher plastic displacement,  $\delta_{\text{plastic}}$ , for the coated grains. The stiffness ratio was observed to decrease consistently for the first four cycles of loading and this explains the faster increase of elastic deformation and decrease of plastic

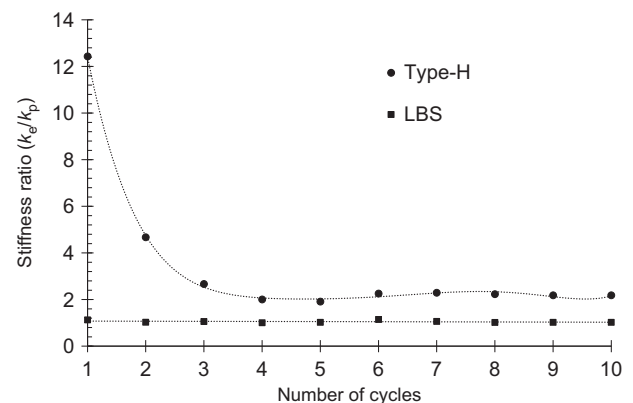


**Fig. 6.** Variation of the stiffness ratio with the number of cycles for type-H and LBS

counterpart (as absolute values as well as portions of the total displacement). Thereafter, not much change was observed in the stiffness ratio (average value of 2.1 was observed) between cycle 4 and cycle 10. For LBS, the stiffness ratio was observed to be constant around 1.1, which shows that the behaviour is purely elastic (Pasha *et al.*, 2014).

#### Elastic and plastic work input (type-H particles)

Work input is defined as the product of the applied force and its corresponding displacement. It was calculated as the total area under the load–displacement curve. As discussed in the section entitled ‘Elastic and plastic deformations’, total displacement can be divided into elastic and plastic fractions, so that the total work done can also be divided into elastic and plastic fractions. To reach a given normal load of 5 N, the work input decreased with increasing number of cycles and reached a stationary value after the completion of a few cycles, as shown in Fig. 7 for type-H particles. After the first cycle of normal load–displacement, the particle contact is no longer softer as in the virgin loading test and this causes the system to have increased values of normal load at a given normal displacement magnitude in subsequent loading cycles. It is also possible that the area of contact between the particles increases with the number of cycles due to the damage of the coating material (see Fig. 4). This increased contact area results in a stiffer contact and decreased work input required to reach a given maximum normal load.

This concept of increase in area of contact is not substantiated by actual numeric values since it is not practically possible to calculate accurately the area of contact after each cycle in a continuous cyclic loading test for coated LBS particles with the available facilities. However, this observation is supported indirectly through Hertzian fitting of Young’s modulus ( $E$ ) to the experimental load–displacement data. It is to be noted that the direct

application of the Hertzian contact model for highly plastic material, such as type-H particles in the present study, is used as an approximation to analyse qualitatively and compare  $E$  values from cycle to cycle for a given contact type. The application of the Hertzian contact model for complex geomaterials is not suitable, owing to the intrinsic simplifications of the model with respect to material properties and contact geometry. Using such models might result in inappropriate values. A few researchers – for example, Nardelli *et al.* (2017) and Sandeep & Senetakis (2018a) – have applied the Hertzian contact model for sand grains. More appropriately, Hanaor *et al.* (2015) showed for rough surfaces an effective method for assessment of contact mechanics by considering asperity–asperity contact. With the aim of qualitative assessment in the present study, for a representative cyclic normal load test, Hertzian fitting was applied and the details of this fitting are shown in Table 2. In this analysis, the local radius at the contact of the particles was calculated from the two-dimensional (2D) projections in two perpendicular directions in the horizontal plane, similarly to the study by Sandeep & Senetakis (2018a), using image analysis. The boundary of the particle in each direction was extracted using the images from digital micro-cameras. The radius of curvature at the possible contact region (apex of the particle) was then estimated. The accuracy of the curvature estimation depends on the resolution or the pixels of the images. The images obtained from the micro-cameras are of high resolution with around 2700 dpi. The particles were carefully chosen using a magnifying glass to avoid any morphological defects in the scale of form and roundness (Zhao & Wang, 2016). Only peak-to-peak contacts were used for the best approximation of local radius. The same local radius calculated before the start of tests was used for fitting all of the data throughout the ten cycles of loading. The variation of  $E$  from cycle 1 to cycle 10 is shown in Fig. 8. It is observed that the  $E$  value for cycle 1 was 5.7 GPa and this is because of the soft kaolinite particle compression. By using the same parameters of fitting as shown in Table 2, for cycle 2 the  $E$  value increased by 8 times (47 GPa) and continued to increase until cycle 10, reaching a maximum  $E$  value of 300 GPa. Increasing stiffness from cycle to cycle as shown in Fig. 5(a) implies an increase in Young’s modulus, but 80–300 GPa is an exceptionally high range of  $E$  values obtained in the last cycles, which are greater than steel and this is not practically possible for sand grains. It is noted that for uncoated quartz grains different values have been reported in the literature by different researchers (e.g. the values reported by Sandeep & Senetakis (2018a, 2018b) are lower compared with the studies by Alshibli *et al.* (2013), Erdoğan *et al.* (2017) and Nardelli & Coop (2018)). In general, within the limitations of the application of the Hertz model, alternative models such as the one proposed by Yimsiri & Soga (2000), which takes into account surface roughness, may work better in the estimation of Young’s modulus (Nardelli & Coop, 2018). It is emphasised that the contact stiffness of rough surfaces is in general stress-dependent (Zhai *et al.*, 2016), so that different stress

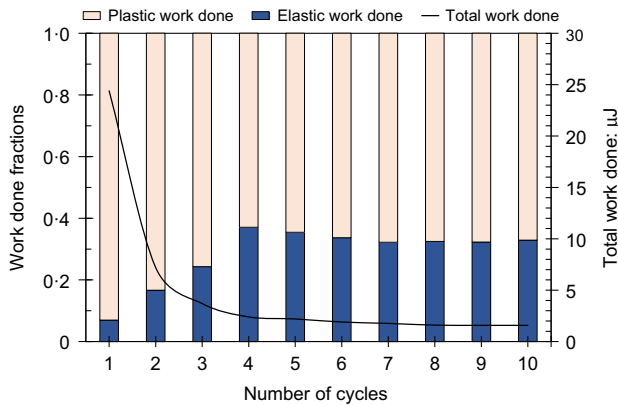


Fig. 7. Fractions of elastic and plastic work done for each cycle and change of the total work done with the number of cycles for type-H particles

Table 2. Details of Hertzian fitting

Test no.	$F_{N,max}$ : N	Cycle	Local radius: mm			Poisson’s ratio, $\nu$	$E = E_1 = E_2$ : GPa	$E^*$ : GPa
			$R_1$	$R_2$	$R^*$			
1	5	1	0.775	0.661	0.357	0.25	7.9	4.2
		2					47.0	25.1
		4					80.0	42.7
		10					300	160

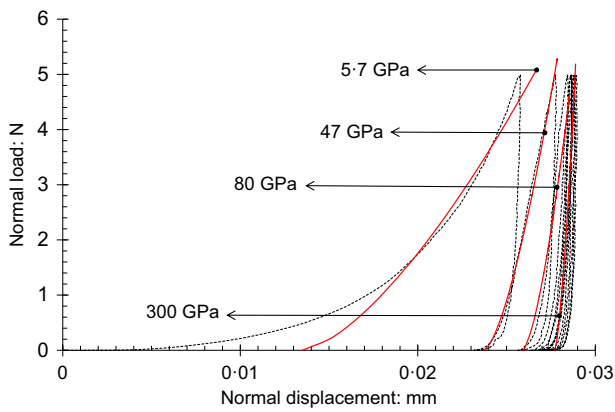


Fig. 8. Hertzian fitting of the normal load–displacement data for type-H particles with same equivalent radius  $R^* = 0.357$  mm for ten cycles

conditions in the experiments can result in these variabilities. Assuming that Hertz fitting is applicable for the current class of materials, it is understood that some parameter(s) should be updated from cycle to cycle to achieve a reasonable range of Young's modulus. By observing the Hertzian equation shown in equation (1), it is understood that the radius of curvature is the main parameter that leads to variable  $E$  values for a given load–displacement curve. This change in curvature during the loading cycles can be physically understood from the compression of the kaolinite particles at the contact region. In the section entitled 'Normal contact stiffness and stiffness ratio', it was mentioned that the contact stiffness was increased due to compression of the kaolinite particles at the contact region. After the application of a normal load, the soft, rounded peaks of the kaolinite-coated LBS grains are damaged and the kaolinite material between the peaks of top and bottom particles is compressed, consequently flattening the contact region with compressed material. This flattened surface of higher curvature becomes the contact region for the successive loading cycles.

$$F_N = \frac{4}{3} (R^*)^{1/2} E^* \delta_N^{3/2} \quad (1)$$

In equation (1),  $R^*$  and  $E^*$  are the equivalent particle radius and equivalent Young's modulus, which are obtained from equations (2) and (3), and  $F_N$  is the normal load corresponding to the normal displacement  $\delta_N$ .

$$R^* = \left( \frac{R_1 R_2}{R_1 + R_2} \right)^{-1} \quad (2)$$

$$E^* = \left( \frac{1 - \nu_1^2}{E_1} + \frac{1 - \nu_2^2}{E_2} \right)^{-1} \quad (3)$$

In equations (2) and (3),  $R$  is the radius of curvature of the particles at the contact (local radius),  $\nu$  and  $E$  are Poisson's ratio and Young's modulus, respectively. The subscripts 1 and 2 denote two particles in contact with each other (top and bottom particles, as shown in Figs 1(b) and 1(c)).

Evidently,  $R^*$  and  $E^*$  are inversely proportional, suggesting that a higher  $R^*$  value must be used in fitting of later cycles to obtain an accurate  $E$  value. With increasing  $R^*$ , the radius of contact ( $a_H$ ) between the particles increases for a given normal load and material type (or  $E^*$ ) according to equation (4). Therefore, an increase in the area of contact with the number of cycles can be indirectly proved and so the work input decreased for a given maximum load. This phenomenon of increased curvature cannot be quantified accurately due to the propagation of damage of the coating

surface around the contact region owing to the peripheral nature of the coating (Kasyap & Senetakis, 2018).

$$a_H = \left( \frac{3F_N R^*}{4E^*} \right)^{1/3} \quad (4)$$

In accordance with the total work input, elastic and plastic work fractions became stationary after a few cycles had been completed (see Fig. 7). In the initial cycles, plastic work done was the dominant, taking up more than 90% of the total work. After four cycles, elastic work input increased to around 35–40% and became steady. The change in displacement was very minimal after the fourth cycle of loading and hence this slight change in displacements could not produce much difference in the total work and consequently in the elastic and plastic work values. Work input calculations for LBS were not performed as the values were very small and it was unrealistic to find the elastic and plastic fractions with precision. The displacement and work input fractions for type-H had a similar trend of high plasticity in the initial cycles and then decreased to a constant value after a few cycles (although different magnitudes). Similar behaviour for LBS could be expected with lower total work input values and higher elastic fractions.

#### Effects of preloading

Figures 9 and 10 show the effect of preloading on the normal load–displacement curves at  $F_N = 5$  N, where the

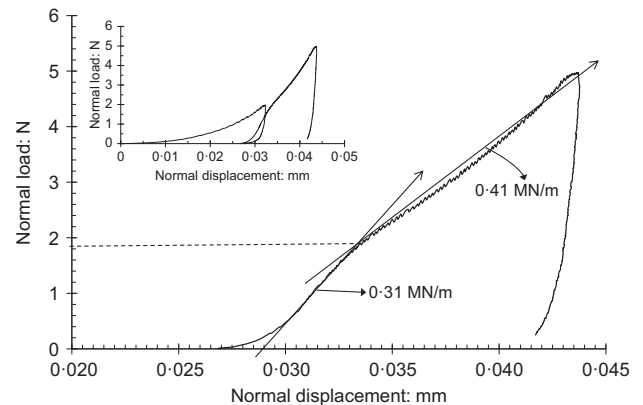


Fig. 9. Change in the behaviour of the normal load–displacement curve for type-H particles at a maximum load of 5 N after the application of a preloading cycle at 2 N. Inset figure shows the complete series of the test

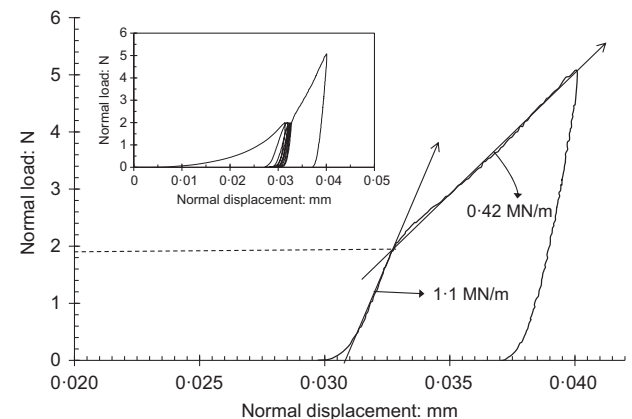


Fig. 10. Change in the behaviour of the normal load–displacement curve for type-H particles at a maximum load of 5 N after the application of five preloading cycles at 2 N. Inset figure shows the complete series of the test

**Table 3.** Summary of the effects of preloading on  $F_N = 5$  N curve

Test no.	Particle type	Preloading condition		Parameters observed		Implications
		Load: N	Cycles	Plastic stiffness, $k_p$	Stiffness ratio	
3	Type-H	2	1	24% decreased after reaching 2 N	—	Elastic behaviour dominates after preloading depending on the normal load and number of preload cycles
4			5	62% decreased after reaching 2 N	—	
5		10	1	No change	Decreased by 69%*	
6	Pure LBS	2	1	Smaller displacement ranges made preloading effects indistinguishable		

\*Compared with the case of 5 N as first cycle  $F_{N,max}$ .

preloading corresponds to one cycle at  $F_N = 2$  N in Fig. 9 and five cycles at  $F_N = 2$  N in Fig. 10. Table 3 provides a summary of the effects of preloading on the normal loading behaviour. In Fig. 9, the normal load–displacement curve at  $F_N = 5$  N showed a shift in plastic stiffness ( $k_p$ ) after it reached 2 N (i.e. reaching the maximum normal load from the previous applied cycle). Specifically, the 5 N loading curve had a slope of 0.41 MN/m until it reached the previous maximum load of 2 N before its slope decreased to 0.31 MN/m. After the applied cycle at  $F_N = 2$  N, the particles experienced a higher level of normal load for the first time and so the compression path changed. In Fig. 10, where the grains experienced five loading cycles at 2 N, the change of the slope of the curve corresponding to the last cycle at 5 N was even greater compared with Fig. 9 (it changed from 1.1 MN/m to 0.42 MN/m when the load reached 2 N). This shows that for a given maximum previous load, the number of cycles has a notable effect on the normal load–displacement behaviour at the grain contacts.

In Fig. 9, the stiffness ratio in the second cycle ( $F_N = 5$  N), after the grains experienced one cycle at  $F_N = 2$  N, is equal to 6.5, approximately. In Fig. 6, the stiffness ratio in the second cycle, after the grains had experienced one cycle at  $F_N = 5$  N, was equal to about 4.7. This means that for a given number of preloading cycles, the stiffness ratio, and thus the portions of elastic and plastic deformation, are influenced by the previous maximum applied normal load for the case of coated sand grains.

A pair of coated grains was tested, similar to the experiment shown in Fig. 9, applying one cycle of 10 N preload and then loading to  $F_N = 5$  N (i.e. the preload was greater than the normal load in the second cycle). No deviations were observed in the 5 N cycle. This demonstrates that significant changes occur in the load–displacement curve (in terms of plastic stiffness and stiffness ratio) only if the preload of a given number of cycles is a lower  $F_N$  than the current load – that is, the particle experiences higher load for the first time. Similar is the case with a higher number of preloading cycles, where no changes are expected if the subsequent cycle after preloading is applied at lower  $F_N$ . It is noted, however, that in the second cycle of the experiment at  $F_N = 5$  N, after the grains had experienced a cycle at  $F_N = 10$  N, the stiffness ratio reached a very low value of 1.4, which implies that elastic deformations were dominant in this case. This indicates that for a given normal load–displacement curve at a given normal load, the stiffness ratio is markedly controlled by the maximum load the grains have experienced. This can lead to an increased stiffness ratio as in the example of Fig. 9, or a notable decrease of the stiffness ratio, as in the previously described case at  $F_N = 10$  N of preloading, as compared to the behaviour shown in Fig. 6. It is understood that, for coated grains, the combination of maximum normal load the grains have experienced compared with the current state as well as the number of previous

loading cycles influences the normal contact behaviour of the grains in terms of stiffness and stiffness ratio, so that elastic and plastic deformations and their fractions are also affected.

For LBS particles, the normal displacements required to reach 5 N load ranged from 2 to 3  $\mu\text{m}$  and hence the effects of preloading were unclear and could not be quantified similarly to type-H particles. Fig. 11 shows the normal load–displacement behaviour of 5 N curve preloaded with 2 N. The significant damage of the coating structure occurring on the surface of type-H particles makes the changes in the behaviour more evident compared with the case of uncoated LBS (see Fig. 4). This can have important implications in DEM modelling, since the level of plastic deformations allowed at the contacts of the grains, considering softer contacts, is notably dependent on the load history. If the simulated problem refers to strong quartz grains with smooth surfaces, the results of the study show that elastic deformations are dominant at the contacts of grains subjected to normal load. If the simulated problem refers to, for example, soil mixtures, where softer particles are present between the sand grains, or in problems related to the simulation of weathered soil/rock profiles, where a coating of clay-to-silt-sized particles may cover the surfaces of the grains, careful consideration must be given to determining elastic and plastic deformations which may be influenced by the previous load history. The direct use of plastic and elastic stiffnesses in order to model the normal contact behaviour of sand grains, as for example the results of Fig. 6, can be easily implemented in a DEM simulation with the compromise that the non-linearity in the force–displacement relationship is not well captured in the loading process. Alternatively, the change of the slope of the normal force–displacement

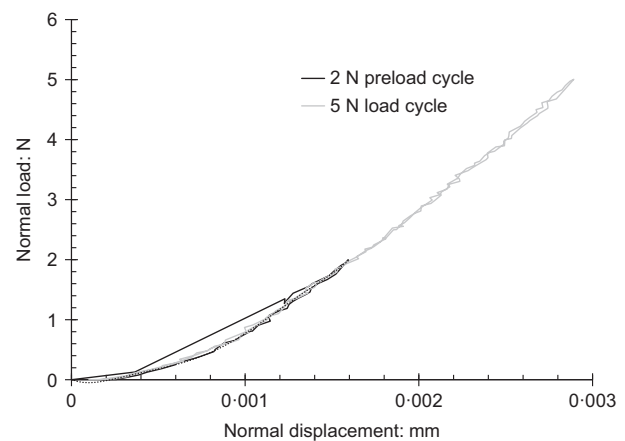


**Fig. 11.** Normal load–displacement curves at a maximum load of 5 N with and without the presence of preloading effects for type-H particles

relationship can be implemented through, for example, the results of Fig. 5, even though these data could provide some upper–lower bounds of behaviour (i.e. very stiff and predominantly elastic behaviour for uncoated and smooth quartz sand grains and very soft behaviour for coated grains, although for soft grains the behaviour will depend also on the loading history).

## CONCLUSIONS

In this study, the normal contact response of uncoated and coated LBS sand grains was studied using a custom-built loading apparatus and the emphasis was placed on the behaviour of the grains subjected to cyclic loading. The coated grains were termed as type-H with heavy coating produced on their surfaces. At a maximum normal load of 5 N, ten cycles of loading and unloading were conducted. Preloading with 2 N and 10 N was conducted to observe their effects on 5 N cycles. Based on the specified testing programme in the study, the following major conclusions are summarised.

- (a) Owing to the compression of soft kaolinite particles, the heavily coated LBS grains (type-H) showed dominant plastic behaviour in the first cycle (90% of total displacements). The behaviour gradually shifted to elastic in nature after four to five cycles. The absolute values of both plastic and total displacements continuously decreased through ten cycles for type-H particles. Uncoated grains (LBS) showed a dominant elastic nature in all of the cycles.
- (b) The peak normal stiffness ( $K_N$ ) values for type-H increased by around 85% through ten cycles of loading. However, after cycle 3 not much variation was observed in  $K_N$ , similarly to the plastic displacement variation. LBS showed a stabilised peak  $K_N$  value of 2.58 MN/m from cycle 1 to cycle 10.
- (c) The stiffness ratio for each cycle was calculated as the ratio of slopes from the unloading curve to the respected loading curve. Type-H particles showed a ratio of 12.4 for cycle 1, indicating very high plastic displacements, and after four cycles the stiffness ratio reached a constant value of around 2.1. LBS showed an average value of 1.1 for all cycles, indicating very high elastic displacements.
- (d) For type-H particles, the work input in reaching a given maximum normal load of 5 N decreased with increasing number of cycles and reached a constant value after four cycles. Minor changes in total displacements could not reflect changes in the work input. The plastic work input fraction decreased, whereas the elastic work fraction increased with the number of cycles.
- (e) For type-H particles, preloading with 2 N instigated a deviation in the normal load–displacement curve of 5 N after reaching 2 N load. The plastic stiffness decreased 25% with one cycle of preloading and 59% with five cycles of preloading. Preloading with 10 N made the subsequent 5 N cycles become stiffer, with elastic displacement becoming dominant. However, the changes in the behaviour of LBS with preloading were unclear, perhaps due to the highly elastic response at the contacts of uncoated grains. In general, it was observed that the combination of the maximum normal load the grain contact had experienced, and the number of previous loading cycles, affect significantly the normal load–displacement curves in terms of stiffness and stiffness ratio.
- (f) Linear models have commonly been adopted in DEM studies owing to their simplicity and consideration of elastic–plastic counterparts (O’Sullivan, 2011). The analysis of the data of this paper adopted such a simple approach, enhanced with the concept of preloading, which seems to be a major influencing factor on the normal contact behaviour. In other words, although a linear model may have some compromises, in a case where such a model is adopted in a numerical study, it should take into account the change of the slope, expressed by the stiffness, due to previous load history. A major contribution of this work is the understanding of the role of number of cycles, preloading and material type considering two extreme cases of pure LBS and soft coated grains, in their normal contact behaviour.

## ACKNOWLEDGEMENTS

The grants from the Research Grants Council of the Hong Kong Special Administrative Region, China, project no. ‘T22-603/15N’ and project ‘CityU 11206617’ are acknowledged for their support to this work.

## NOTATION

$a_H$	radius of contact between particles
$E$	Young’s modulus
$E^*$	equivalent Young’s modulus
$F_N$	normal load
$F_{N-max}$	maximum normal load reached in a test
$K_N$	normal contact stiffness
$K_{N1}^H$	normal contact stiffness of type-H grains under $F_N = 1$ N
$K_{N10}^H$	normal contact stiffness of type-H grains under $F_N = 10$ N
$K_{N1}^{LBS}$	normal contact stiffness of uncoated LBS grains under $F_N = 1$ N
$K_{N10}^{LBS}$	normal contact stiffness of uncoated LBS grains under $F_N = 10$ N
$k_e$	elastic stiffness
$k_p$	plastic stiffness
$R$	radius of curvature of particles at the contact
$R^*$	equivalent particle radius
$S_q$	surface roughness
$\delta_{elastic}$	elastic deformation
$\delta_{N-max}$	maximum normal displacement reached under $F_{N-max}$
$\delta_{plastic}$	plastic deformation
$\delta_{total}$	total deformation
$\nu$	Poisson’s ratio

## REFERENCES

- Alshibli, K., Cil, M. B., Kenesei, P. & Lienert, U. (2013). Strain tensor determination of compressed individual silica sand particles using high-energy synchrotron diffraction. *Granular Matter* **15**, No. 5, 517–530.
- Barrows, H. L., Simpson, E. C. & Tu, H. Y. (1966). Formation of surface coatings on limestone particles in soil. *Soil Sci. Soc. Am. Proc.* **30**, No. 3, 318–320.
- Cavarretta, I., Coop, M. R. & O’Sullivan, C. (2010). The influence of particle characteristics on the behaviour of coarse grained soils. *Géotechnique* **60**, No. 6, 413–423, <https://doi.org/10.1680/geot.2010.60.6.413>.
- Cole, D. M. & Hopkins, M. A. (2016). The contact properties of naturally occurring geological materials: experimental observations. *Granular Matter* **18**, No. 3, article 62.
- Cole, D. M. & Peters, J. F. (2007). A physically based approach to granular media mechanics: grain-scale experiments, initial results, and implications to numerical modelling. *Granular Matter* **9**, No. 5, 309–321.
- Cole, D. M. & Peters, J. F. (2008). Grain-scale mechanics of geologic materials and lunar simulants under normal loading. *Granular Matter* **10**, No. 3, 171–185.

- Cundall, P. A. & Strack, O. D. L. (1979). A discrete numerical model for granular assemblies. *Géotechnique* **29**, No. 1, 47–65, <https://doi.org/10.1680/geot.1979.29.1.47>.
- Dai, B. B., Yang, J. & Zhou, C. Y. (2016). Observed effects of inter-particle friction and particle size on shear behavior of granular materials. *Int. J. Geomech.* **16**, No. 1, 04015011.
- Erdogan, S. T., Forster, A. M., Stutzman, P. E. & Garboczi, E. J. (2017). Particle-based characterization of Ottawa sand: shape, size, mineralogy, and elastic moduli. *Cem. Concr. Compos.* **83**, 36–44.
- Hanaor, D., Gan, Y. & Einav, I. (2015). Contact mechanics of fractal surfaces by spline assisted discretization. *Int. J. Solids Structs* **59**, 121–131.
- Huang, X., Hanley, K. J., O'Sullivan, C. & Kwok, C. Y. (2017). Implementation of a rotational resistance models: a critical appraisal. *Particuology* **34**, 14–23.
- Kasyap, S. S. & Senetakis, K. (2018). A micromechanical experiments of kaolinite-coated sand grains. *Tribol. Int.* **126**, 206–217.
- Kawamoto, R., Ando, E., Viggiani, G. & Andrande, J. E. (2018). All you need is shape: predicting shear banding in sand with LS-DEM. *J. Mech. Solids* **111**, 375–392.
- Luding, S. (2008). Cohesive, frictional powders: contact models for tension. *Granular Matter* **10**, No. 4, 235–246.
- Nardelli, V. & Coop, M. R. (2018). The experimental contact behaviour of natural sands: normal and tangential loading. *Géotechnique* **69**, No. 8, 672–686, <https://doi.org/10.1680/jgeot.17.P167>.
- Nardelli, V., Coop, M. R., Vitone, C. & Chen, S. (2016). The inter-scale behaviour of two natural scaly clays. *Géotechnique Lett.* **6**, No. 3, 205–210, <https://doi.org/10.1680/jgele.16.00060>.
- Nardelli, V., Coop, M. R., Andrade, J. E. & Paccagnella, F. (2017). An experimental investigation of the micromechanics of Eglin sand. *Powder Technol.* **312**, 166–174.
- O'Sullivan, C. (2011). Particle-based discrete element modelling: geomechanics perspective. *Int. J. Geomech.* **11**, No. 6, 449–464.
- Otsubo, M. & O'Sullivan, C. (2018). Experimental and DEM assessment of the stress-dependency of surface roughness effects on shear modulus. *Soils Found.* **58**, No. 3, 602–614.
- Pasha, M., Dogbe, S. & Hare, C. (2014). A linear model of elasto-plastic and adhesive contact deformation. *Granular Matter* **16**, No. 1, 151–162.
- Phan, V. T., Hsiao, D. H. & Nguyen, P. T. L. (2016). Effects of fines contents on engineering properties of sand-fines mixtures. *Procedia Engng* **142**, 213–220.
- Sandeep, C. S. & Senetakis, K. (2018a). Grain-scale mechanics of quartz sand under normal and tangential loading. *Tribol. Int.* **117**, 261–271.
- Sandeep, C. S. & Senetakis, K. (2018b). Effect of Young's modulus and surface roughness on the inter-particle friction of granular materials. *Mater. (Basel)* **11**, No. 2, article 217.
- Sandeep, C. S. & Senetakis, K. (2019). An experimental investigation of the microslip displacement of geological materials. *Comput. Geotech.* **107**, 55–67.
- Sandeep, C. S., Todisco, M. C., Nardelli, V., Senetakis, K., Coop, M. R. & Lourenco, S. D. N. (2018). A micromechanical experimental study of highly/completely decomposed tuff granules. *Acta Geotechnica* **13**, No. 6, 1355–1367.
- Sazzad, M. M. & Suzuki, K. (2011). Effect of interparticle friction on the cyclic behavior of granular materials using 2D DEM. *J. Geotech. Geoenviron. Engng* **137**, No. 5, 545–549.
- Scheidegger, A., Borkovec, M. & Sticher, H. (1993). Coating of silica sand with goethite: preparation and analytical identification. *Geoderma* **58**, No. 1–2, 43–65.
- Senetakis, K. & Coop, M. R. (2014). The development of a new micro-mechanical inter-particle loading apparatus. *Geotech. Test. J.* **37**, No. 6, 1028–1039.
- Senetakis, K., Coop, M. & Todisco, M. C. (2013). The inter-particle coefficient of friction at the contacts of Leighton Buzzard sand quartz minerals. *Soils Found.* **53**, No. 5, 746–755.
- Soga, K. & O'Sullivan, C. (2010). Modeling of geomaterials behavior. *Soils Found.* **50**, No. 6, 861–875.
- Thornton, C. (2000). Numerical simulations of deviatoric shear deformation of granular media. *Géotechnique* **50**, No. 1, 43–53, <https://doi.org/10.1680/geot.2000.50.1.43>.
- Todisco, M. C., Wang, W., Coop, M. R. & Senetakis, K. (2017). Multiple contact compression tests on sand particles. *Soils Found.* **57**, No. 1, 126–140.
- Walton, O. R. & Johnson, S. M. (2009). Simulating the effects of interparticle cohesion in micron-scale powders. *AIP Conference Proceedings* **1145**, No. 1, 897–900.
- Wang, W., Nardelli, V. & Coop, M. R. (2017). Micro-mechanical behaviour of artificially cemented sands under compression and shear. *Géotechnique Lett.* **7**, No. 3, 218–224, <https://doi.org/10.1680/jgele.16.00166>.
- Wang, W., Coop, M. R. & Senetakis, K. (2018). The development of a micro-mechanical apparatus applying combined normal-shear-bending forces to natural sand grains with artificial bonds. *Geotech. Test. J.* **42**, No. 4, 1090–1099.
- Yang, J. & Wei, L. M. (2012). Collapse of loose sand with addition of fines: the role of particle shape. *Géotechnique* **62**, No. 12, 1111–1125, <https://doi.org/10.1680/geot.11.P062>.
- Yimsiri, S. & Soga, K. (2000). Micromechanics-based stress-strain behaviour of soils at small strains. *Géotechnique* **50**, No. 5, 559–571, <https://doi.org/10.1680/geot.2000.50.5.559>.
- Zhai, C., Gan, Y., Hanaor, D., Proust, G. & Retraint, D. (2016). The role of surface structure in normal contact stiffness. *Expl Mech.* **56**, No. 3, 359–368.
- Zhao, B. & Wang, J. (2016). 3D quantitative shape analysis on form, roundness, and compactness with  $\mu$ CT. *Powder Technol.* **291**, 262–275.